Star-QAM Constellation Design for Hierarchically Modulated PON Systems With 20-Gbps PSK and 10-Gbps OOK Signals

Naotaka Shibata, Noriko Iiyama, Jun-ichi Kani, *Member, IEEE*, Sang-Yuep Kim, Jun Terada, *Member, IEEE*, and Naoto Yoshimoto, *Senior Member, IEEE*

***Abstract*—In this paper, we show an effective star-QAM constellation in terms of the allowable range of the extinction ratio for hierarchically modulated PON systems that overlay a 20-Gbps PSK signal on a 10-Gbps OOK signal. In ten-star and 17-star QAM signals, the modulation level of the PSK signal is dynamically changed based on the amplitude of the OOK signal while the modulation level of the PSK signal is constant in the fundamental eight-star QAM signal. Numerical results studied the performance of these constellations, and indicated the effective constellation to achieve the lowest power penalty depends on the extinction ratio. Simulation results showed that by using eight-star QAM or ten-star QAM signals, new ONUs satisfied the required receiver sensitivity in 10G-EPON and XG-PON. Experimental results showed that, compared to the eight-star QAM signal, the ten-star QAM signal enhanced the range of the extinction ratio wherein ONUs of legacy and new systems satisfied the required sensitivity for 10G-EPON and XG-PON. The range was from 7.4 –9.7 dB. The ten-star QAM signal also improved the required received power by 7.7 dB compared to the required sensitivity in 10G-EPON when the extinction ratio was 8.2 dB.**

***Index Terms*—Co-existence, coherent detection, hierarchical modulation, high-order modulation, passive optical network (PON).**

I. Introduction

A HIGHER bandwidth is required if passive optical networks (PONs) are to support future bandwidth demand from, for example, mobile backhaul/fronthaul [1], [2]. PON systems, such as 10G-EPON and XG-PON, offer 10 Gbps capacity. This capacity can be improved in proportion to the number of wavelengths by using multi-wavelength techniques. The wavelength band available to new systems is a very limited resource, so the efficient use of each wavelength is required [3]. High-order modulation is a promising technique to further improve the capacity for the next-generation multi-wavelength PON systems. High-order modulation provides higher spectral efficiency while the receiver sensitivity is improved by using coherent detection.

Manuscript received April 24, 2014; revised July 3, 2014; accepted July 13, 2014. Date of publication July 20, 2014; date of current version August 13, 2014. This work was supported in part by the U.S. Department of Commerce under Grant BS123456.

N. Shibata, N. Iiyama, J.-i. Kani, S. Y. Kim, and J. Terada are with the NTT Access Network Service Systems Laboratories, NTT Corporation, Kanagawa 239–0847, Japan (e-mail: shibata.naotaka@lab.ntt.co.jp).

N. Yoshimoto is with the Chitose Institute of Science and Technology, Hokkaido 066–8655, Japan (e-mail: n-yoshi@photon.chitose.ac.jp).

Color versions of one or more of the figures in this paper are available online at http://ieeexplore.ieee.org.

Digital Object Identifier 10.1109/JLT.2014.2341239

Hierarchical modulation, which consists of multiple layers in a high-order modulation signal, allows the simultaneous downlink transmission from one optical line terminal (OLT) to multiple optical network units (ONUs) [4]–[6]. Hierarchical modulation can be used during the migration period to achieve the co-existence of legacy ONUs that use on-off keying (OOK) modulation and new ONUs that use high-order modulation on the same PON branch [4], [5]. Hereafter, we call the PON system where the legacy and new ONUs coexist by using hierarchical modulation as the hierarchically-modulated PON system (HM-PON). In this system, the OLT transmits a star quadrature amplitude modulation (QAM) signal in which a phase-shift keying (PSK) signal is multiplexed with an OOK signal in a wavelength. The legacy ONUs can receive the data from the OOK signal while the new ONUs receive the data from the OOK and PSK signals. In HM-PON, an OLT can support, during the migration period, both legacy and new ONUs on the same PON branch with a wavelength.

Previous investigations confirmed the feasibility of HM-PON employing an eight-star QAM signal with a 30.5-dB loss budget [4]. In eight-star QAM signals, the modulation level of the PSK signal is constant. The performance of the PSK signal degrades as the extinction ratio increases because the bit error rate (BER) of the PSK signal with lower amplitude (inner-PSK signal) degrades. For realizing HM-PON in higher extinction ratios, we proposed other constellations where the modulation level of the PSK signal is dynamically changed based on the amplitude of the OOK signal [5]: The modulation level of the inner-PSK signal is reduced to improve the BER of new ONUs while maintaining the average transmission rate by increasing the modulation level of the PSK signal with higher amplitude (outer-PSK signal). The previous work showed that the effective constellation design in terms of the maximum receiver sensitivity depends on the extinction ratio by computer simulation [5]. It is necessary to evaluate how much the allowable extinction ratio in legacy systems is enhanced by dynamically changing the modulation level of the PSK signal compared to the fundamental eight-star QAM signal.

In this paper, we extend previous work [5] on constellation designs for HM-PON that overlay a 20-Gbps PSK signal on a 10-Gbps OOK signal as follows. In Section II, the system model is described in more detail, including buffer controls when the modulation level of the PSK signal is dynamically changed. In Section III, a numerical analysis is newly performed to evaluate the performance of PSK parts in three types of constellations.

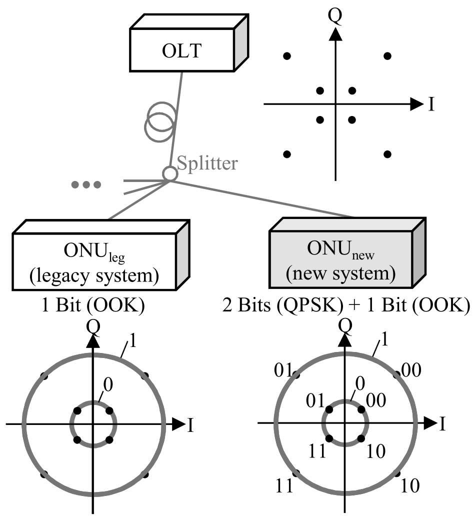

Fig. 1. HM-PON using eight-star QAM signal.

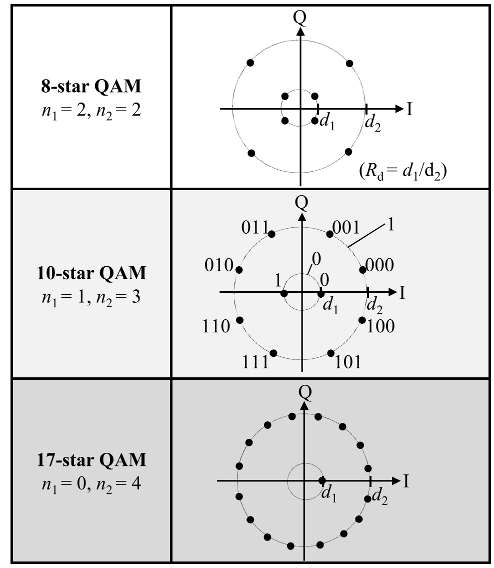

Fig. 2. Star-QAM constellations for HM-PON.

In Section IV, we evaluate these constellations by simulations in terms of the allowable range of the extinction ratio in addition to the receiver sensitivity, adjusting the simulation parameters to fit minimum or typical values in experimental devices. In Section V, experiments are newly performed to evaluate the extinction ratio range wherein both legacy and new ONUs satisfy the required sensitivity.

II. System Model

A. Concept of HM-PON

Fig. 1 shows the HM-PON using an eight-star QAM signal [4]. The new ONUs using high-order modulation, $\mathrm{ONU_{new}}$, coexist with the legacy ONUs using OOK modulation, $\mathrm{ONU_{leg}}$, on the same PON branch. In downlink transmission, the data for $\mathrm{ONU_{leg}}$, $\mathrm{data_{leg}}$, and the data for $\mathrm{ONU_{new}}$, $\mathrm{data_{new}}$, are simultaneously transmitted with a wavelength by an OLT using a star QAM signal. In a star QAM signal, a PSK signal based on $\mathrm{data_{new}}$ is multiplexed with an OOK signal based on $\mathrm{data_{leg}}$. $\mathrm{ONU_{new}}$ receives OOK and PSK parts via coherent detection while $\mathrm{ONU_{leg}}$ receives only the OOK part via direct detection. The OOK part can be used to transmit $\mathrm{data_{new}}$ in addition to the PSK part. In the following, we assume that bit "1" of $\mathrm{data_{leg}}$ corresponds to the high amplitude of the OOK signal.

B. Constellations for HM-PON

Fig. 2 shows the star-QAM constellations considered in this paper. The amplitudes of the OOK signal are defined as d_1 and d_2 ($d_1 < d_2$). We define R_d as d_1/d_2. The modulation level of the inner-PSK signal is defined as 2^{n1}, and that of the outer-PSK signal as 2^{n_2}.

In this paper, we study three types of constellations: eight-star QAM ($n_1 = n_2 = 2$), ten-star QAM ($n_1 = 1, n_2 = 3$), and 17-star QAM ($n_1 = 0$, $n_2 = 4$) [5]. The eight-star QAM signal is evaluated for comparison with ten- and 17-star QAM signals. The modulation level of the PSK signal is dynamically changed based on $\mathrm{data_{leg}}$ in ten- and 17-star QAM signals. In the 17-star QAM signal, only the outer-PSK signal is used to transmit $\mathrm{data_{new}}$. Let us define R_{sym} as the symbol rate of the transmitted signal. In all the constellations, the average transmission rate of the PSK part is expected to be $2R_{\mathrm{sym}}$ since the use of line coding makes the probability of bit "0" and "1" in $\mathrm{data_{leg}}$ approximately the same. The average transmission rate of $\mathrm{ONU_{new}}$ is expected to be $3R_{\mathrm{sym}}$ when both the OOK and PSK parts are used to transmit $\mathrm{data_{new}}$.

C. Block Diagram

Fig. 3 shows block diagrams of the OLT and $\mathrm{ONU_{new}}$ when $n_1 < n_2$ as in ten- and 17-star QAM signals [5]. The OLT and $\mathrm{ONU_{new}}$ employ digital signal processing (DSP) techniques. In the OLT, some bits of $\mathrm{data_{new}}$ are stored in the buffer for delay of $T_{\mathrm{del}}/R_{\mathrm{sym}}$ before transmitting $\mathrm{data_{new}}$. The controller changes the number of bits output from the buffer based on whether the input of $\mathrm{data_{leg}}$ is "0" or "1." That is, n_1 bits are read out from the buffer when the input of the controller is bit "0," and n_2 bits are read out when the input of the controller is bit "1." The bit-to-symbol mapper (star-QAM) outputs star-QAM signals based on $\mathrm{data_{leg}}$ and $\mathrm{data_{new}}$.

A star-QAM signal is received by coherent detection at $\mathrm{ONU_{new}}$. In $\mathrm{ONU_{new}}$, the received signals are OOK demodulated, and sorted into inner-PSK signals and outer-PSK signals at the symbol-to-bit demapper (OOK). These signals are compensated for phase drift due to frequency offset at the phase compensator, PSK demodulated at the symbol-to-bit demapper, and stored in the buffer. The controller changes the output from the switch based on $\mathrm{data_{leg}}$, and rearranged $\mathrm{data_{new}}$ is obtained at $\mathrm{ONU_{new}}$. If there are errors in $\mathrm{data_{leg}}$ obtained by OOK demodulation, the symbol-to-bit demapper (OOK) cannot sort the input signals correctly. Therefore, the BER of $\mathrm{data_{new}}$ degrades as the BER of $\mathrm{data_{leg}}$ degrades.

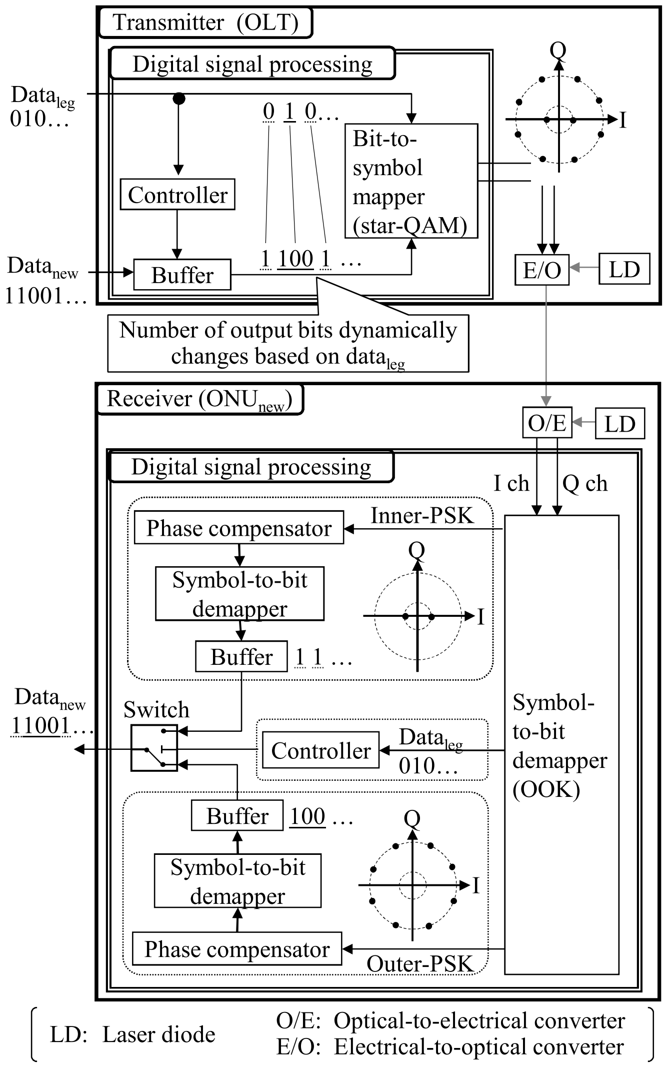

Fig. 3. Block diagrams of OLT and $\mathrm{ONU_{new}}$ employing ten-star QAM signal.

When $n_1 = n_2$ as in the eight-star QAM signal, controllers, buffers, and the switch are removed from OLT and $\mathrm{ONU_{new}}$, and only one set, comprising phase compensation and symbol-to-bit demapper for a PSK signal, is required at $\mathrm{ONU_{new}}$. Thus, the BER of $\mathrm{data_{new}}$ is independent of that of $\mathrm{data_{leg}}$.

D. Buffer Size

The size of the buffer in the OLT, B_{size}, is estimated for ten- and 17-star QAM signals. When the input of the controller in the OLT is bit “1,” the number of bits in the OLT buffer is reduced. This is because the output rate from the buffer of $n_2 R_{\mathrm{sym}}$ is higher than the input rate to the buffer of $2R_{\mathrm{sym}}$. Therefore, some bits of $\mathrm{data_{new}}$ have to be stored in $T_{\mathrm{del}}/R_{\mathrm{sym}}$ to avoid a buffer empty condition due to a sequence of “1” bits. If the input of the controller in the OLT is bit “0,” the number of bits in the buffer is increased. This is because the output rate from the buffer of $n_1 R_{\mathrm{sym}}$ is lower than the input rate to the buffer of $2R_{\mathrm{sym}}$. Therefore, B_{size} must be sufficiently large to avoid a buffer overflow condition caused by a series of “0” bits. Let us define N_0 and N_1 as the total number of “0 s” and “1s” input to the controller, respectively. The required B_{size} increases as the difference between N_0 and N_1 increases.

The required B_{size} is reduced by line coding such as 8B/10B and 64B/66B since the difference between N_0 and N_1 is reduced. When $\mathrm{data_{leg}}$ is 8B/10B encoded, $\max(N_1 - N_0)$ and $\max(N_0 - N_1)$ are limited to 3 [7]. First, T_{del} must satisfy the following equation to avoid the buffer empty condition,

$$T_{\mathrm{del}}(n_1 + n_2)/2 > \max(N_1 - N_0)\{n_2 - (n_1 + n_2)/2\}. \tag{1}$$

The 17-star QAM signal incurs the maximum delay among the constellations in Fig. 2 and $T_{\mathrm{del}} > 3$. Second, B_{size} must satisfy the following equation to avoid the buffer overflow condition,

$$T_{\mathrm{del}}(n_1 + n_2)/2 + \max(N_0 - N_1) \\ \{(n_1 + n_2)/2 - n_1\} < B_{\mathrm{size}}. \tag{2}$$

The 17-star QAM signal requires the maximum buffer size among the constellations in Fig. 2 and $B_{\mathrm{size}} > 12$ bits. In a similar way, the required buffer sizes for the inner-PSK and outer-PSK signals of $\mathrm{ONU_{new}}$ are given as $3n_1$ bits and $3n_2$ bits, respectively.

The required B_{size} is also reduced by adjusting the number of bits stored in the buffer. The number of bits in the buffer is reduced by temporarily reducing or stopping the input of $\mathrm{data_{new}}$ to the buffer, and is increased by inserting dummy data of $\mathrm{data_{new}}$ into the buffer. The dummy data is detected and discarded at $\mathrm{ONU_{new}}$. Another method is to insert a dummy data frame into $\mathrm{data_{leg}}$ in Layer 2. The dummy data frame contains a larger number of “0 s” or “1 s” in Layer 1 to reduce or increase the number of bits in the buffer. The MAC address of the dummy frame is set not to indicate any ONU, so that the frame is discarded by all ONUs. Therefore, the buffer overflow and empty conditions are avoided when the number of bits stored in the buffer is adjusted by these methods.

III. Numerical Evaluations

A. Numerical Model

The performance of each constellation design was numerically evaluated. The BER performance of the modulated signal depends heavily on the minimum distance between constellation points. The minimum distance between constellation points of the OOK part is $1 - R_d$, which is normalized by d_2. The minimum distance between constellation points of the inner-PSK part is $2R_d \sin(\pi/2^{n_1})$, and that of the outer-PSK part is $2\sin(\pi/2^{n_2})$. We define $d_{\min,i}$ as the minimum distance that has the greatest impact on the BER of the PSK part in *i*-star QAM signals (i = 8, 10, 17). Distance $d_{\min,i}$ is given as

$$d_{\min,8} = 2R_d \sin(\pi/4) \tag{3}$$

$$d_{\min,10} = \min\{2\sin(\pi/8), 2R_d, 1 - R_d\} \tag{4}$$

$$d_{\min,17} = \min\{2\sin(\pi/16), 1 - R_d\}. \tag{5}$$

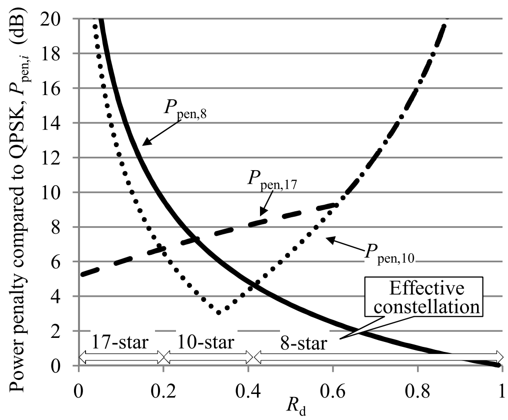

Fig. 4. Numerical evaluation of effective constellation depending on R_d.

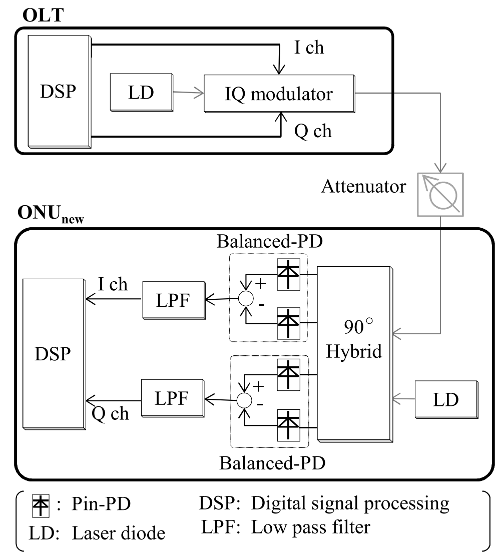

Fig. 5. Simulation configuration.

.

In the eight-star QAM signal, $1 - R_d$ is removed since the BER of the PSK part is independent of that of the OOK signal, and 2sin(π/4) is removed since it is larger than $2R_d\sin(\pi/4)$. In the 17-star QAM signal, $2R_d\sin(\pi/2^{n_1})$ is removed since the inner-PSK signal is not used for transmission. The power penalty for *i*-star QAM signals compared to a quadrature PSK (QPSK) signal, $P_{\mathrm{pen},i}$, is given as

$$P_{\mathrm{pen},i} = 20\log_{10}\left(\sqrt{2}/d\min,i\right) + 20\log_{10}\{(1+R_d)/2\}[\mathrm{dB}]. \tag{6}$$

Here, $20\log_{10}\{(1+R_d)/2\}$ equalizes the average power of the modulated signals at any R_d.

B. Numerical Results

Fig. 4 plots $P_{\mathrm{pen},i}$ as a function of R_d. Penalty $P_{\mathrm{pen},8}$ increases as R_d decreases since $d_{\min,8}$ is $2R_d\sin(\pi/4)$ at any R_d. Penalty $P_{\mathrm{pen},10}$ decreases as R_d decreases from 1 to 0.33, and $P_{\mathrm{pen},10}$ increases as R_d decreases from 0.33 to 0. This implies that $d_{\min,10}$ is $1 - R_d$ when $R_d > 0.33$ and $d_{\min,10}$ is $2R_d$ when $R_d < 0.33$. $P_{\mathrm{pen},17}$ decreases as R_d decreases from 1 to 0.61 since $d_{\min,17}$ is $1 - R_d$. Comparatively, $P_{\mathrm{pen},17}$ decreases slightly as R_d decreases from 0.61 to 0 since $20\log_{10}\{(1+R_d)/2\}$ decreases while $d_{\min,17}$ is constant, 2sin(π/16). For example, the ten-star QAM signal improves the power penalty by 3 dB compared to the eight-star QAM signal when $R_d < 0.33$. Fig. 4 shows that the effective constellation design, i.e., the design that achieves the lowest power penalty, depends on R_d. The effective constellation is eight-star QAM when $R_d > 0.41$, ten-star QAM when $0.41 > R_d > 0.2$, and 17-star QAM when $R_d < 0.2$.

IV. Simulations

A. Simulation Model

Simulations were performed to evaluate the performance of constellations in eight-, ten-, and 17-star QAM signals. Fig. 5 shows the simulation configuration, and Table I summarizes the simulation parameters. DSP blocks in Fig. 5 are the same as those in Fig. 3. $\mathrm{ONU_{new}}$ receives signals by coherent detection using 90° optical hybrid and balanced-PDs. The OLT uses an IQ modulator. We define $\mathrm{ER_{sig}}$ as the extinction ratio of the modulated optical signal, i.e., the ratio of the average power of the outer-PSK signal to that of the inner-PSK signal. $\mathrm{ER_{sig}}$ is obtained from the signal at the output of the IQ modulator. We also define $\mathrm{ER_{MZM}}$ as the maximum extinction ratio of the Mach-Zehnder modulator (MZM) in the IQ modulator, and $\mathrm{ER_{sig}}$ is limited to $\mathrm{ER_{MZM}}$. $\mathrm{ER_{MZM}}$ was set to 20 or 35 dB. 20 dB is the minimum guaranteed value for the IQ modulator used in the following experiments, and 35 dB is sufficiently high to modulate signals in eight-, ten-, and 17-star QAM signals with negligible signal distortion. In the following simulations and experiments, $\mathrm{data_{leg}}$ and $\mathrm{data_{new}}$ comprise a pseudo-random bit sequence (PRBS) of length $2^{15} - 1$. The initial bit sequence of the PRBS of $\mathrm{data_{leg}}$ is all-1 bits. In a PRBS sequence of length $2^{15} - 1$, $\max(N_1 - N_0) = 15$, and $\max(N_0 - N_1) = 235$, so the 17-star QAM signal requires that $T_{\mathrm{del}} > 15$ and $B_{\mathrm{size}} > 500$ bits.

TABLE I
Simulation Parameters

LDs of OLT and $\mathrm{ONU_{new}}$	
Wavelength band	1550 nm
Frequency offset	1 MHz
Transmit power	10 dBm
Line width	100 kHz
PD	
Responsivity	0.8 A/W
Dark current	20 nA
Low pass filter	Third-order Bessel filter (Cutoff frequency = 7.5 GHz)
Phase compensation	Mth power algorithm [8]
Symbol rate, $\mathrm{R_{sym}}$	10 Gsymbol/s
Maximum extinction ratio of MZM, $\mathrm{ER_{MZM}}$	20 dB, 35 dB
Required BER of $\mathrm{data_{leg}}$ and $\mathrm{data_{new}}$	10^{-3}

We define P_{req} as the minimum required received power where the PSK part satisfies the required BER. We evaluated P_{req} in back-to-back transmissions. In the eight-star QAM signal, the required BER of data$_{\mathrm{new}}$ is satisfied with higher sensitivity than P_{req}. In ten- and 17-star QAM signals, the required BERs of data$_{\mathrm{leg}}$ and data$_{\mathrm{new}}$ are satisfied with higher sensitivity than P_{req}. It was assumed that when the OOK part met the required BER, data$_{\mathrm{leg}}$ was correctly decoded and the symbol-to-bit demapper (OOK) sorted the input signals into inner- and outer-PSK signals correctly. The required BER in data$_{\mathrm{leg}}$ and data$_{\mathrm{new}}$ were set to 10^{-3}. Rate R_{sym} rate was set to 10 Gsymbol/s, so the average transmission rate of the OOK part was 10 Gbps and that of the PSK part was 20 Gbps in all the constellations. The simulation parameters are set to fit minimum or typical values in the devices such as LDs and PDs used in the following experiments, unlike previous studies [5]. This caused the difference between the results in this paper and those of the previous work [5].

B. Simulation Results

Fig. 6(a) plots P_{req} as a function of the target R_d when ER$_{\mathrm{MZM}}$ is 35 dB. The target R_d means that DSP block in the OLT adjusts parameters and outputs the signal so that ER$_{\mathrm{sig}}$ is set to $20\log_{10}(1/R_d)$ when the star-QAM signals are modulated with no signal distortion. In the eight-star QAM signal, P_{req} increases as the target R_d decreases as in numerical results. In the ten-star QAM signal, P_{req} decreases as the target R_d decreases from 0.5 to 0.3 since the BER of the OOK part improves, and P_{req} increases as the target R_d decreases from 0.3 to 0.1 since the BER of the inner-PSK part degrades. Using the 17-star QAM signal, P_{req} slightly decreases as the target R_d decreases because reducing the target R_d improves the received power of the outer-PSK signals at a given average received power. The most effective constellation, i.e., the design that achieves the lowest P_{req}, is eight-star QAM when the target $R_d > 0.44$, ten-star QAM when $0.44 >$ the target $R_d > 0.17$, and 17-star QAM when the target $R_{\mathrm{d}} < 0.17$. Ten-star QAM, for example, improves P_{req} by 4 dB compared to eight-star QAM when the target R_d is between 0.3 and 0.17. The simulation results with 35-dB ER$_{\mathrm{MZM}}$ are similar to the numerical results in terms of the improvement when using ten-star QAM and the effective range of the target R_d in each constellation.

Fig. 6(b) plots P_{req} as a function of the target R_d when ER$_{\mathrm{MZM}}$ is 20 dB. The low ER$_{\mathrm{MZM}}$ compared to Fig. 6(a) led to the transmitted signal distortion [9] and the degradation of P_{req}. In particular, P_{req} in eight- and ten-star QAM signals significantly degrades as the target R_d decreases because the effect of this signal distortion is large for the inner-PSK signals. The most effective constellation is eight-star QAM when the target $R_d > 0.41$, ten-star QAM when $0.41 >$ the target $R_d > 0.19$, and 17-star QAM when the target $R_d < 0.19$. The improvement when using ten-star QAM is larger than that in Fig. 4 and Fig. 6(a) under some conditions on the target R_d. Ten-star QAM, for example, improves P_{req} by 7 dB compared to eight-star QAM when the target $R_d = 0.25$. This implies that reducing n_1 is very effective in improving the BER of the inner-PSK signal compared to the results from the numerical evaluation.

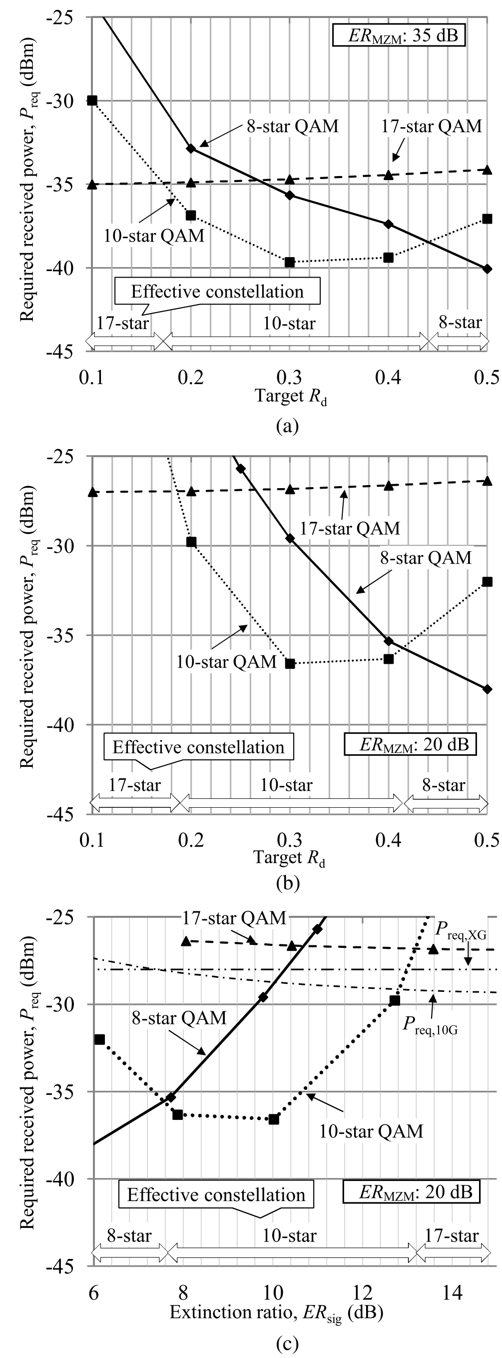

Fig. 6. (a) Simulation of constellation effectiveness versus target R_d (ER$_{\mathrm{MZM}}$ = 35 dB). (b) Simulation of constellation effectiveness versus target R_d (ER$_{\mathrm{MZM}}$ = 20 dB). (c) Simulation of constellation effectiveness versus extinction ratio, ER$_{\mathrm{sig}}$ (ER$_{\mathrm{MZM}}$ = 20 dB).

Fig. 6(c) plots P_{req} as a function of ER$_{\mathrm{sig}}$ when ER$_{\mathrm{MZM}}$ is 20 dB. ER$_{\mathrm{sig}}$ in Fig. 6(c) deviated from $20\log_{10}(1/R_d)$ due to the signal distortion caused by the low ER$_{\mathrm{MZM}}$: for example, when the target R_d was 0.3 in ten-star QAM, ER$_{\mathrm{sig}}$ was 10 dB while $20\log_{10}(1/0.3) = 10.5$ dB. The required receiver sensitivity in XG-PON, $P_{\mathrm{req,XG}}$, is -28 dBm, and that in 10G-EPON,

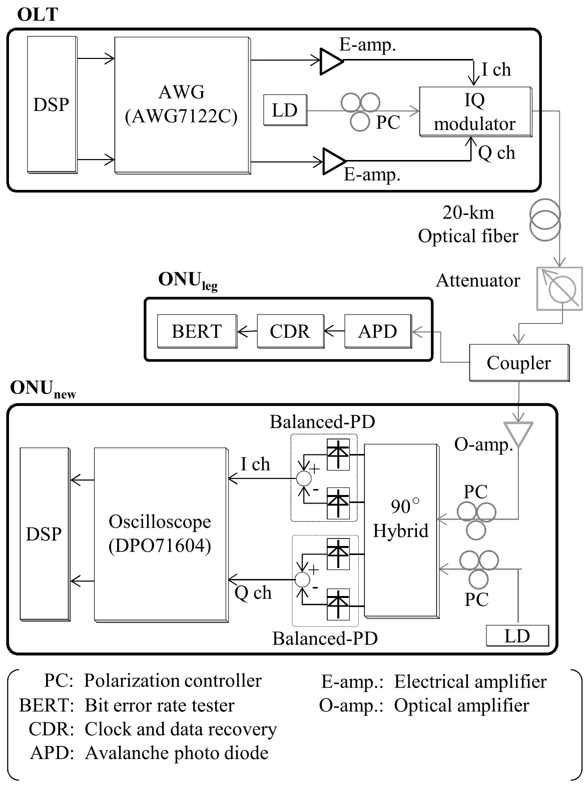

Fig. 7. Experimental configuration.

$P_{\mathrm{req,10G}}$, is calculated using the receiver sensitivity optical modulation amplitude and $\mathrm{ER_{sig}}$ [10], [11]. For example, $P_{\mathrm{req,10G}}$ is −28.3 dBm when $\mathrm{ER_{sig}}$ is 8.2 dB. Eight- and ten-star QAM signals meet $P_{\mathrm{req,XG}}$ and $P_{\mathrm{req,10G}}$ for a certain range of $\mathrm{ER_{sig}}$. The upper limit of the range was 10 dB in eight-star QAM, and 12.8 dB in ten-star QAM. Compared to eight-star QAM, ten-star QAM enhances the upper limit of the $\mathrm{ER_{sig}}$ where $\mathrm{ONU_{new}}$ satisfies $P_{\mathrm{req,XG}}$ and $P_{\mathrm{req,10G}}$. The minimum $\mathrm{ER_{sig}}$ for the 10G-EPON and XG-PON is 6 and 8.2 dB, respectively [10], [11], and the transmitters are generally implemented with a margin for the minimum $\mathrm{ER_{sig}}$. Therefore, ten-star QAM enhances the applicability of HM-PON since the allowable margin in the legacy system is improved. In the following experiments, 17-star QAM is not evaluated since $\mathrm{ONU_{new}}$ doesn't satisfy $P_{\mathrm{req,XG}}$ and $P_{\mathrm{req,10G}}$. If new systems provide only relatively short-distance transmissions, HM-PON can be applicable for higher $\mathrm{ER_{sig}}$ than 12.8 dB, and 17-star QAM achieves the lowest P_{req} in higher $\mathrm{ER_{sig}}$ than 13.2 dB.

V. EXPERIMENTS

A. Experimental Configuration

Experiments were conducted to confirm the feasibility of the ten-star QAM signal and evaluate the improvement in performance when using ten-star QAM compared to eight-star QAM. Fig. 7 shows the experimental model, and Table II summarizes the parameters used in experiments. An Arbitrary Waveform Generator (Tektronix AWG7122C) was used as the digital-to-analog converter. A real-time oscilloscope (DPO 71604) was used as the analog-to-digital converter. Ratio $\mathrm{ER_{sig}}$ was measured by using a communications signal analyzer (Tektronix CSA-8000B). DSP blocks in Fig. 7 are the same as those in Fig. 3. Offline DSP was performed using a PC. The required BER in $\mathrm{data_{leg}}$ and $\mathrm{data_{new}}$ were set to 10^{-3}. Rate R_{sym} was set to 10 Gsymbol/s, so the average transmission rate of the OOK part was 10 Gbps, and that of the PSK part was 20 Gbps in all the constellations. In addition to P_{req} of the PSK part, P_{req} of the OOK part at $\mathrm{ONU_{leg}}$ was evaluated to confirm that $\mathrm{ONU_{leg}}$ can receive $\mathrm{data_{leg}}$ with lower sensitivity than $P_{\mathrm{req,XG}}$ and $P_{\mathrm{req,10G}}$. We investigated the performance of back-to-back transmission and 20-km transmission. Radius directed equalization (RDE) was used to compensate for the distortion due to 20-km transmission [12].

TABLE II
EXPERIMENTAL PARAMETERS

LDs of OLT and $\mathrm{ONU_{new}}$	
Wavelength band	1550 nm
Frequency offset	< 1 MHz
Transmit power	10 dBm
Line width	< 100 kHz
PD	
Responsivity	> 0.7 A/W
Dark current	< 50 nA
3-dB bandwidth	> 12 GHz
Phase compensation	Mth power algorithm [8]
Symbol rate, R_{sym}	10 Gsymbol/s
IQ modulator	
Maximum extinction ratio of MZM, $\mathrm{ER_{MZM}}$	> 20 dB
3-dB bandwidth	> 22 GHz
Required BER of $\mathrm{data_{leg}}$ and $\mathrm{data_{new}}$	10^{-3}

B. Experimental Results

Fig. 8(a) plots P_{req} as a function of $\mathrm{ER_{sig}}$ with back-to-back transmission. For the same target R_d, $\mathrm{ER_{sig}}$ in Fig. 8(a) decreased compared to the simulation results due to the signal distortion at the analog devices of the transmitter. For example, the target $R_d = 0.4$ of ten-star QAM leads to $\mathrm{ER_{sig}} = 7.74$ dB in the simulation results but $\mathrm{ER_{sig}} = 6.06$ dB in the experimental results. The OOK parts in eight- and ten-star QAM signals exhibited almost the same performance. $\mathrm{ONU_{leg}}$ met $P_{\mathrm{req,XG}}$ and $P_{\mathrm{req,10G}}$ when $\mathrm{ER_{sig}} > 7.3$ dB. Ten-star QAM outperformed eight-star QAM in terms of P_{req} when $\mathrm{ER_{sig}} > 6$ dB. Compared to eight-star QAM, ten-star QAM enhanced the upper limit of $\mathrm{ER_{sig}}$ where $\mathrm{ONU_{new}}$ meet $P_{\mathrm{req,XG}}$ and $P_{\mathrm{req,10G}}$ as in the case of the simulation results. The upper limit was 9.8 dB in ten-star QAM while it was 8.1 dB in eight-star QAM.

Fig. 8(b) shows the eye diagram output from the IQ modulator and constellation diagrams of received signals at $\mathrm{ONU_{new}}$ when the received power was −28 dBm and the transmission distance was 0 km. The figure shows that the amplitude of the inner-PSK signal relatively decreases compared to that of the outer-PSK signal as $\mathrm{ER_{sig}}$ increases. The minimum distance between constellation points of the inner-PSK improved with the use of ten-star QAM.

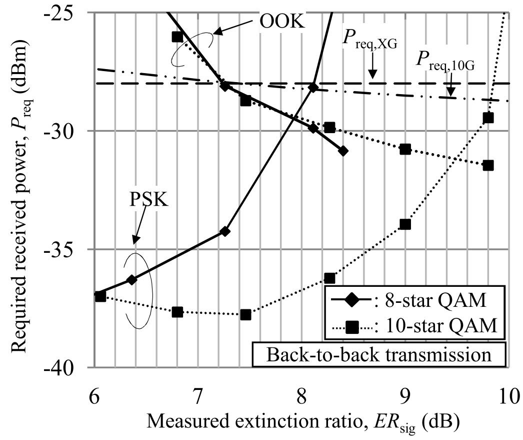

(a)

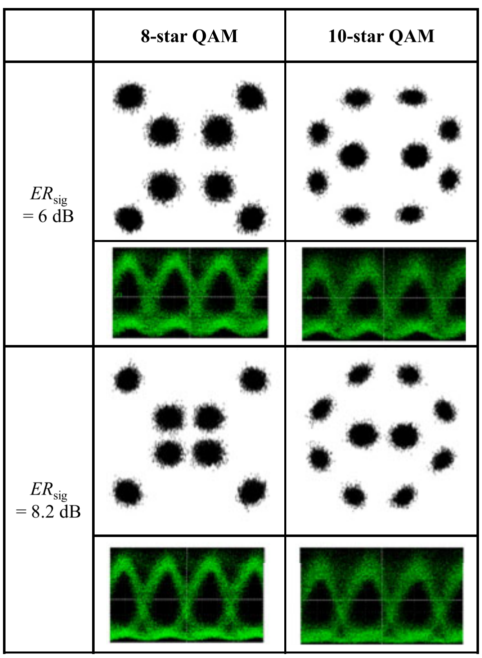

(b)

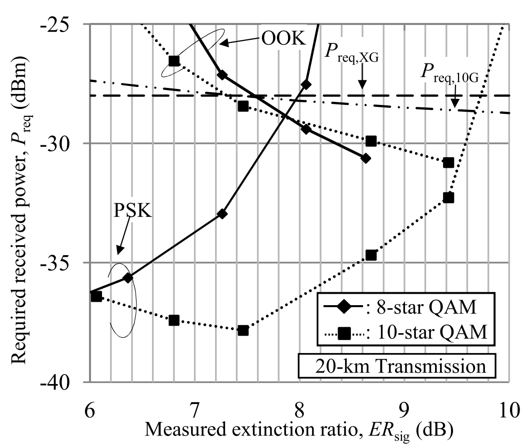

(c)

Fig. 8. (a) Experimental results of required received power versus measured extinction ratio (back-to-back transmission). (b) Constellation diagrams of received signals at the $\mathrm{ONU}_{\mathrm{new}}$ when the received power was -28 dBm and eye diagrams output from IQ modulator. (c) Experimental results of required received power versus measured extinction ratio (20-km transmission).

Fig. 8(c) plots P_{req} as a function of $\mathrm{ER}_{\mathrm{sig}}$ with 20-km transmission. The RDE compensated for the signal distortion caused by the 20-km transmission, and it resulted in a slightly narrower range of $\mathrm{ER}_{\mathrm{sig}}$ where $\mathrm{ONU}_{\mathrm{leg}}$ and $\mathrm{ONU}_{\mathrm{new}}$ satisfied $P_{\mathrm{req,XG}}$ and $P_{\mathrm{req,10G}}$: The range was 7.6 to 7.8 dB in eight-star QAM, and 7.4 to 9.7 dB in ten-star QAM. Ten-star QAM enhanced the applicability of HM-PON in terms of providing a wider range of $\mathrm{ER}_{\mathrm{sig}}$, and outperformed eight-star QAM in terms of P_{req}. Compared to $P_{\mathrm{req,10G}}$, P_{req} in ten-star QAM was improved by 9.8 and 7.7 dB when $\mathrm{ER}_{\mathrm{sig}}$ was 7.5 and 8.2 dB, respectively.

VI. Conclusion

In this paper, we studied the performance of three types of star-QAM signals for the HM-PON by numerical analysis, simulations, and experiments. Numerical evaluations showed that the effective constellation to achieve the lowest power penalty depends on the extinction ratio. Simulation results showed that eight-star QAM and ten-star QAM signals satisfy $P_{\mathrm{req,XG}}$ and $P_{\mathrm{req,10G}}$. Finally, experiments showed the feasibility of the ten-star QAM signal. Also, the ten-star QAM signal enhanced the extinction ratio range where $\mathrm{ONU}_{\mathrm{leg}}$ and $\mathrm{ONU}_{\mathrm{new}}$ satisfy $P_{\mathrm{req,XG}}$ and $P_{\mathrm{req,10G}}$. The range was 7.4 to 9.7 dB while that for the fundamental eight-star QAM signal was 7.6 to 7.8 dB. The ten-star QAM signal improved the required received power by 7.7 dB compared to $P_{\mathrm{req,10G}}$ when the extinction ratio was 8.2 dB.

References

[1] J. Kani, F. Bourgart, A. Cui, A. Rafel, M. Campbell, R. Davey, and S. Rodrigues, "Next-generation PON-part I: Technology roadmap and general requirements," *IEEE Commun. Mag.*, vol. 47, no. 11, pp. 43–49, Nov. 2009.

[2] N. Cvijetic, A. Tanaka, M. Civijetic, Y.-K. Huang, E. Ip, Y. Shao, and T. Wang, "Novel optical access and digital processing architecture for future mobile backhaul," *J. Lightw. Technol.*, vol. 31, no. 4, pp. 621–627, Feb. 2013.

[3] F. J. Effenberger, H. Mukai, J.-I. Kani, and M. Rasztovits-Wiech, "Next-generation PON part III: System specifications for XG-PON," *IEEE Commun. Mag.*, vol. 47, no. 11, pp. 58–64, Nov. 2009.

[4] N. Iiyama, J. Kani, J. Terada, and N. Yoshimoto, "Feasibility study on a scheme for coexistence of DSP-based PON and 10-Gbps/λ PON using hierarchical star QAM format," *J. Lightw. Technol.*, vol. 31, no. 18, pp. 3085–3092, Sep. 2013.

[5] N. Shibata, N. Iiyama, J. Kani, S. Y. Kim, J. Terada, and N. Yoshimoto, "Constellation design for next-generation hierarchically-modulated PON systems," *Proc. SPIE*, vol. 8645, p. 864507, Feb. 2013.

[6] P. Cao, X. Hu, Z. Zhuang, L. Zhang, Q. Chang, Q. Yang, R. Hu, and Y. Su, "Power margin improvement for OFDMA-PON using hierarchical modulation," *Opt. Exp.*, vol. 21, no. 7, pp. 8261–8268, Apr. 2013.

[7] A. X. Widmer and P. A. Franaszek, "A DC-balanced, portioned lock, 8B/10B transmission code," *IBM J. Res. Develop.*, vol. 27, no. 5, pp. 440–451, Sep. 1983.

[8] M. Seimetz, *High-Order Modulation For Optical Fiber Transmission*. New York, NY, USA: Springer, 2009.

[9] T. Kawanishi, T. Sakamoto, A. Chiba, and M. Izutsu, "Study of precise optical modulation using Mach-Zehnder interferometers for advanced modulation formats," in *Proc. 33rd Eur. Conf. Exhib. Opt. Commun.*, 2007, pp. 1–2.

[10] ITU-T Recommendation G.987.2, "10-Gigabit-capable passive optical networks (XG-PON): Physical media dependent (PMD) layer specification," Oct. 2010.

[11] *Carrier Sense Multiple Access With Collision Detection (CSMA/CD) Access Method and Physical Layer Specification, Amendment 1: Physical Layer Specifications and Management Parameters for 10 Gbit/s Passive Optical Networks*, IEEE Standard 802.3av, Oct. 2009.

[12] I. Fatadin, D. Ives, and S. J. Savory, "Blind equalization and carrier phase recovery in a 16-QAM optical coherent system," *J. Lightw. Technol.*, vol. 27, no. 15, pp. 3042–3049, Aug. 2009.

Naotaka Shibata received the B.E. degree in electrical and electronic engineering and the M.E. degree in communications and computer engineering from Kyoto University, Kyoto, Japan, in 2007 and 2009, respectively.

In 2009, he joined the NTT Access Network Service Systems Laboratories, where he was involved in the research of wireless communication systems. Since 2012, his research interests include optical-wireless converged networks.

Mr. Shibata is a Member of the Institute of Electronics, Information, and Communication Engineers, Japan.

Noriko Iiyama received the B.E. degree in system design engineering and the M.E. degree in integrated design engineering from Keio University, Kanagawa, Japan, in 2006 and 2008, respectively.

Since 2008, she has been with the NTT Access Network Service Systems Laboratories, where her research interests include optical access networks and systems.

Ms. Iiyama is a Member of the Institute of Electronics, Information, and Communication Engineers, Japan. She received the Best Paper Award from the 18th Optoelectronics and Communications Conference in 2013.

Jun-ichi Kani (M'98) received the B.E., M.E., and Ph.D. degrees all in applied physics from Waseda University, Tokyo, Japan, in 1994, 1996, and 2005, respectively.

In 1996, he joined the NTT Optical Network Systems Laboratories, where his research interests include optical multiplexing and transmission technologies. Since 2003, he has been with the NTT Access Network Service Systems Laboratories, where he is involved in the research and development of optical communication systems for metro and access applications.

Dr. Kani is a Member of the Institute of Electronics, Information, and Communication Engineers. He has been participating in ITU-T and the Full Service Access Network initiative, since 2003, and is serving as an Associate Rapporteur of the ITU-T Q2/15 (optical systems for fiber access networks) since 2009.

Sang-Yuep Kim received the Ph.D. degree in electronics engineering from Kwangwoon University, Seoul, Korea, in 2004. From 2004 to 2007, he was with the University of Tokyo, Japan, under a Postdoctoral Foreign Researcher Fellowship.

In 2008, he joined NTT Access Network Service Systems Laboratories, NTT Corporation, Chiba, Japan. He is currently researching DSP technologies for future optical access systems.

Jun Terada (M'02) received the B.E. degree in science and engineering and M.E. degree in computer science from Keio University, Kanagawa, Japan, in 1993 and 1995, respectively.

In 1995, he joined the NTT LSI Laboratories, where he was involved in research and development of low-voltage analog circuits, especially A/D and D/A converters. From 1999, he was involved in developing small- and low-power wireless systems for sensor networks. From 2006, he was involved in high-speed front-end circuits for optical transceivers. He is currently a Senior Research Engineer and a Supervisor with the NTT Access Network Service Systems Laboratories, where he is responsible for the R&D management of optical and wireless converged access networks.

Mr. Terada is a Member of the Institute of Electronics, Information and Communication Engineers of Japan, and he has served as a Member of technical program committee of Symposium on Very Large Scale Integration Circuit and is currently serving the Asian Solid- State Circuits Conference, since 2012.

Naoto Yoshimoto (M'94–SM'14) received the B.S., M.S., and Ph.D. degrees in electronics and information engineering from Hokkaido University, Japan, in 1986, 1988, and 2003, respectively. He is a Senior R&D Manager at NTT Laboratories.

He joined NTT Laboratories in 1988, and is involved in the research and development of optical transmission equipment and related optical modules for broadband access systems, and in the planning and design of next-generation optical access networks and architectures mainly based on high-speed TDM-PON and future advanced PON technologies. In particular, he has recently been devoting effort to advanced research for resilient broadband access networks using microwave-photonic convergence technologies. From 2014, he is a Professor with the Chitose Institute of Science and Technology.

Dr. Yoshimoto is a Senior Member of the IEEE Communication Society, Optical Society of America, and Institute of Electronics, Information and Communication Engineers of Japan.